Article

Optimizing Sustainable Energy Generation in Ethanol Fuel Cells: An Exploration of Carrageenan with TiO$_2$ Nanoparticles and Ni/CeO$_2$ Composites

Ermides Chavez-Baldovino,* Carlos A. Malca-Reyes, Roberto Masso, Peter Feng, Adrian Camacho, Janeth Sarmiento, Justin I. Borrero Negrón, Yomaira J. Pagán-Torres, and Liz M. Díaz-Vázquez*

Read Online

ACCESS | Metrics & More | Article Recommendations

ABSTRACT: Based on the search for new biodegradable materials that are low cost and easy to synthesize by environmentally friendly methods, we report the use of carrageenan membranes (mixture of κ and λ carrageenans) with different concentrations of titanium dioxide nanoparticles (TiO$_2$ NPs) and Ni/CeO$_2$ (10 wt % Ni) for the fabrication of a novel fuel cell electrode for the oxidation of ethanol. Each membrane was characterized to determine its physicochemical properties using X-ray diffraction (XRD), differential scanning calorimetry (DSC), and Fourier transform infrared (FTIR) spectroscopy. Using impedance spectroscopy (IS), a maximum value of 2.08×10^{-4} S/cm in ionic conductivity was found for the carrageenan nanocomposite with a concentration of 5 wt % TiO$_2$ NPs (CR5%). Due to its high conductivity values, the CR5% membrane was mixed with Ni/CeO$_2$ to prepare the working electrode for cyclic voltammetry measurements. Using a solution of 1 M ethanol and 1 M KOH, the oxidation of ethanol over CR5% + Ni/CeO$_2$ resulted in peak current density values at forward and reverse scan voltages of 9.52 and 12.22 mA/cm^2, respectively. From our results, the CR5% + Ni/CeO$_2$ membrane proves to be more efficient in the oxidation of ethanol compared with commercially available Nafion membranes containing Ni/CeO$_2$.
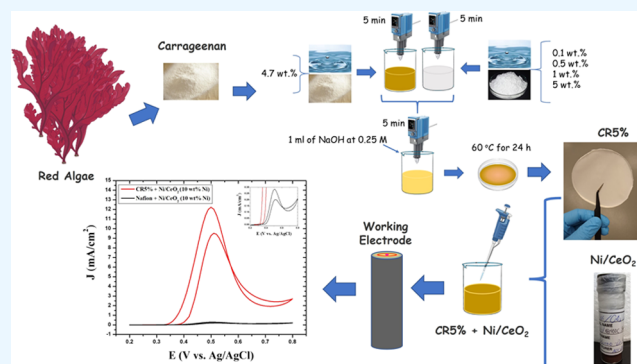
1. INTRODUCTION

In recent years, polymers have been widely studied as an alternative in the production of electronic devices, capacitors, and fuel cells.[1,2] However, there is a problem with their low biodegradability, which causes a harmful impact on the environment and health.[2,3] For this reason, it is necessary to find new materials that are more environmentally friendly, which generates the need to obtain new materials as substitutes for these polymers and meet eco-friendly expectations.[3,4] One of the alternatives to solve this problem is the use of natural polymers or biopolymers that are abundantly found in nature and inexpensive. These also have specific physical and chemical properties that make them good candidates to replace synthetic polymers.[5] Several investigations have been carried out on these biopolymers, especially on carrageenan, which is a family of sulfated polysaccharides whose main polysaccharide chain is mainly formed by the β-D-galactopyranose monomers and α-D-galactopyranose linked through α-(1 → 3) and β-(1 → 4) bonds.[6,7] Furthermore, there are nanoparticles of metal oxides, such as titanium dioxide nanoparticles (TiO$_2$ NPs), which have specific physicochemical characteristics that make them good candidates as additives in biopolymers since they

have been shown to be biocompatible, nontoxic, and cheap, with dielectric properties.[8,9]

Several research groups have been working with nanocomposites of biopolymers mixed with metal oxides and other compounds. For example, Lizundia et al.[10] prepared nanocomposites of poly(L-lactide) (PLLA) with cellulose nanocrystals (CNC), which showed reduction on thermal stability when in the presence of CNC-grafted-PLLA, while raw CNC slightly increases the thermal stability of PLLA. Shukur et al.[11] found an increase in the conductivity of 1.04×10^{-3} S/cm with addition of glycerol on corn starch-based solid biopolymer electrolytes doped with lithium acetate (LiOAc). On the other hand, Ng and Camacho[12] prepared a polymer electrolyte blend composed of a mixture of poly(3,4-ethylene dioxythiophene) (PEDOT) and κ-carrageenan for application in dye-sensitized

solar cells. Jo et al.[13] studied cellulose/carrageenan/TiO$_2$ nanoparticles nanocomposites and the efficiency of adsorption and photodegradation for methyl blue.

Contrary to these biopolymers, there are synthetic polymers, such as polyfluorinated sulfonic acid ionomers (for example, Nafion),[14] which are used worldwide in the manufacture of fuel cells for the generation of clean energy. However, it has been reported in recent decades that polyfluorinated substances' widespread presence in the environment is correlated with adverse effects on human health and ecology.[15,16] To mitigate part of this problem, in this study, we performed a detailed analysis of the thermal, electrical, and structural properties of membranes made of mixed (κ and λ) carrageenan (biopolymer) with TiO$_2$ NPs (CR5%). In addition, Ni/CeO$_2$ was incorporated as a catalyst to CR5% to study the performance of these materials in the oxidation of ethanol (alkaline media) through cyclic voltammetry measurements. The Ni/CeO$_2$ catalysts were used since cerium-based metal oxides have been reported to exhibit excellent redox properties.[17,18] Our results show that CR5% + Ni/CeO$_2$ exhibits a higher efficiency in the oxidation of ethanol compared with commercially available Nafion membranes containing Ni/CeO$_2$ under equivalent conditions.

2. MATERIALS AND METHODS

2.1. Materials. Titanium dioxide (TiO$_2$) nanoparticles (TiO$_2$ NPs) with a purity of 99.5% and particle size of approximately 21 nm; mixed carrageenan (κ and λ); ethanol (99.5%); sodium hydroxide (NaOH 99.99%); potassium hydroxide (KOH, 99.99%); and Nafion perfluorinated resin solution 5 wt % in lower aliphatic alcohols−water mix were used. All reagents were used without modification and purchased from Sigma-Aldrich. Glassy carbon (GC) electrodes (3.0 mm diameter) from Bio-Analytical Systems (B.A.S.) were used as working electrodes. The deionized water used for the experiments was previously distilled and pumped through a Nanopure system (Barnstead) to give a resistivity of 18.2 MΩ· cm.

2.2. Synthesis of the Samples. The procedure to obtain the nanocomposites was very similar to that of Lizundia et al.,[4,10] with a few minor modifications. A polysaccharide solution of 4.7 wt % was prepared by mixing 5 ± 0.01 of carrageenan and 100 mL of distilled water. Then, 1 mL of sodium hydroxide solution (NaOH) at 0.25 mol/L was added and dispersed (n T 18 B S1 ULTRA-TURRAX disperser was used, with an output power of 40% to homogenize the mixture). Subsequently, in different beakers, with a volume of 25 mL of distilled water, the TiO$_2$ NPs were dispersed with a concentration of 0.1, 0.5, 1, and 5 wt % (labeled as CR0.1%, CR0.5%, CR1%, and CR5%, respectively) and stirred for 5 min with an output power of 16.0%. To these samples of dispersed TiO$_2$ NPs, 15 ± 0.01 g of carrageenan solution at 4.7 wt % and NaOH were added, and then the mixture was stirred for 5 min, with an output power of 40%. Then, the final mixture was placed in different Petri dishes at 65 °C for 24 h.

The Ni/CeO$_2$ (10 wt % Ni) catalyst was prepared by incipient wetness impregnation of an aqueous solution of nickel (II) nitrate hexahydrate (Alfa-Aesar, 98%) on cerium oxide (donated by Daiichi Kigenso Kagaku Kogyo Co., Ltd). The obtained powder was dried overnight at 393 K, followed by calcination at 400 °C for 3 h at a ramp rate of 5 °C/min under flowing dried air at 40 mL/min.

2.3. Differential Scanning Calorimetry (DSC). To study the thermal stability of the samples, a Mettler Toledo DSC 822e calorimeter was used. Nanocomposites of approximately 6 ± 1 mg in aluminum capsules and dry nitrogen were used as a purge gas, with a flow rate of 60 mL/min and a heating rate of 5 °C/min from room temperature to 500 °C.

2.4. X-ray Diffraction (XRD). The crystalline structures of the samples were studied using a Rigaku X-ray diffractometer (Smartlab) with a Cu Kα monochromatic radiation source. Data were collected from 20 to 80° with a sampling step of 0.02° and a scanning speed of 1°/min.

2.5. Fourier Transform Infrared Spectroscopy (FTIR). Fourier transform infrared spectroscopy measurements (FTIR) were recorded by a Shimadzu IRAffinity-1S spectrophotometer coupled with an attenuated total reflectance cell (ATR). The measurements were carried out in a range of 400−4000 cm^{-1} with 100 scans and a resolution of 2 cm^{-1}.

2.6. Impedance Spectroscopy (IS). The electrical measurements of the nanocomposites were made with the help of a HIOKI 3522-50 L.C.R. impedance analyzer (Hioki E. E. Corporation, Melrose, MA) in the frequency range of 42−5 MHz at room temperature.

2.7. Scanning Electron Microscopy (SEM). Surface morphology was examined using a scanning electron microscope (SEM). The micrographs were taken on a JSM-6360 (JEOL, Japan) with an acceleration voltage of 8 kV and a working distance of 8 mm. The observation was conducted at room temperature.

2.8. Cyclic Voltammetry Measurements (CV). For the electrochemical characterization, cyclic voltammetry was used through a PalmSens4 potentiostat with a traditional three-electrode cell composed of a glassy carbon working electrode (GCE), a platinum wire as an auxiliary electrode, and an Ag/AgCl as a reference electrode. The GCE was modified with different CR, CR5%, and CR5% + Ni/CeO$_2$ (10 wt % Ni) solutions and different Nafion and Nafion + Ni/CeO$_2$ (10 wt % Ni) solutions. The measurements were made at room temperature in solutions containing 10 mL of 1 M KOH, and another with 10 mL of 1 M KOH with 1 M ethanol at a scan rate of 100 mV/s in a range of −1.4 to 1.4 V.

2.8.1. Characterization of Working Electrodes. The procedure used to prepare the G.C. working electrodes was very similar to that used by Feliciano-Ramos et al.,[19] with some minor modifications. The working electrode alone (bare) was initially run. The surface of the working electrode was polished with 5 μm alumina and washed several times with ultrapure water to place on it 5 μL of carrageenan solution (CR) (5 mg in 10 mL of ultrapure water), which was then placed to air-dry for 30 min. This procedure was repeated for the CR5% membranes. We made a slight variation for the CR5% + Ni/CeO$_2$ (10 wt % Ni) membrane, where we mixed 5 mg of Ni/CeO$_2$ (10 wt % Ni) with 2.5 mL of ethanol and 80 μL CR5% solution (5 mg in 10 mL of ultrapure water) and sonicated it for 30 min. An analogous procedure was used for the Nafion membrane. Initially, the working electrode alone was run, then the working electrode with the Nafion solution, and finally, we ran the Nafion solution with Ni/CeO$_2$ (10 wt % Ni). All of these measurements were made first in a 1 M KOH solution and another with 1 M KOH with 1 M ethanol solution at a scan rate of 100 mV/s over a range of −1.4 to 1.4 V.

2.8.2. Assembly of the Working Electrode with CR5% and Nafion in the Modification of Glassy Carbon (GC) Electrodes. For the first electrode, we mixed 5 mg Ni/CeO$_2$ (10 wt %

Ni) with 2.5 mL of ethanol and 80 μL of CR5% solution (5 mg in 10 mL of ultrapure water) and sonicated the mixture for 30 min. On the surface of the working electrode, 5 μL of CR5% + Ni/CeO$_2$ (10 wt % Ni) solution was placed to air-dry for 30 min at room temperature. For the second electrode, the procedure was similar, but this time, 80 μL of Nafion solution was used instead of the CR5% solution over a range of 0.2−0.8 V.

2.9. Energy Dispersive X-ray Spectroscopy (EDX). Energy dispersive X-ray spectroscopy measurements were conducted in a scanning electron microscope (SEM). The spectra were taken on a JSMIT-500 HR (JEOL, Japan), with an accelerating voltage of 20 kV and a working distance of 10 mm. All spectra were taken at room temperature.

3. RESULTS AND DISCUSSION

After the synthesis process of the nanocomposites, different characterization measurements were carried out on the
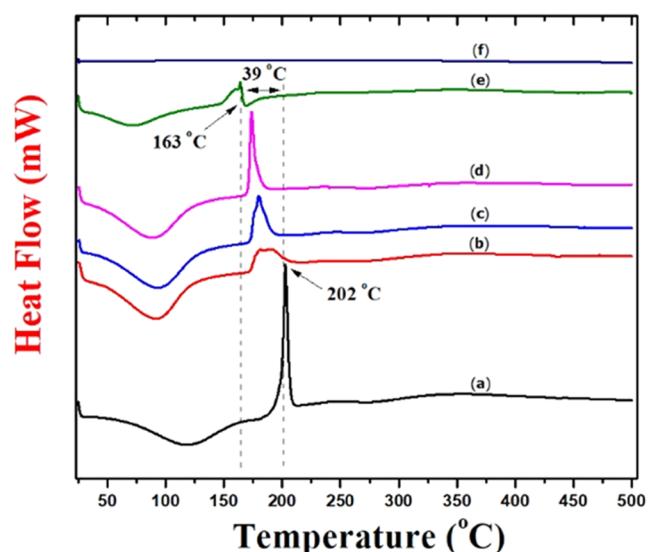
Figure 1. DSC thermogram showing the thermal stability of the samples: (a) carrageenan (CR), (b) carrageenan with a concentration of 0.1 wt % of TiO$_2$ NPs (CR0.1%), (c) carrageenan with a concentration of 0.5 wt % of TiO$_2$ NPs (CR0.5%), (d) carrageenan with a concentration of 1 wt % of TiO$_2$ NPs (CR1%), (e) carrageenan with a concentration of 5 wt % of TiO$_2$ NPs (CR5%), and (f) pure TiO$_2$ NPs.

samples to know their thermal, structural, electrical, and morphological properties and to determine their potential application in the electro-oxidation of ethanol compared to the membrane, widely used commercially, as is the Nafion.

3.1. Thermal Stability of Nanocomposites. It is necessary to know the thermal stability of the materials to determine their limit-operating temperatures and, in this way, to know the range of temperatures where they can be used, for this reason. Figure 1 shows the DSC thermogram for different nanocomposites and their precursors (mixed carrageenan (κ and λ) and TiO$_2$ nanoparticles). Two thermal anomalies are observed in the carrageenan and the four composites (CR0.1%, CR0.5%, CR1%, and CR5%). The first anomaly corresponds to an endothermic peak observed around 100 °C, belonging to the water physically bound in the composites and carrageenan. Similar behavior in the κ-carrageenan was reported before.[14,16,17] A second anomaly is observed around 200 °C,[20]

which corresponds to an exothermic peak. It could be associated with a crystalline phase or decomposition process in the different composites. The exothermic peak obtained in this study matched the data previously reported by Prasad et al.[21] in the three types of carrageenans (κ, ι, and λ). A shift of the exothermic peak was observed toward lower temperatures as the concentration of TiO$_2$ particles increased. This shift reflects a change in the thermal properties of the carrageenan, probably due to structural changes of the nanocomposites. On the other hand, TiO$_2$ NPs do not present any thermal anomaly due to their thermal stability over a wide range of temperatures.[9] To better investigate the hypothesis of whether there is any structural change in the composites due to the variation of TiO$_2$ NPs, X-ray diffraction measurements were made.

3.2. Change of the Structure of the Samples. The X-ray measurement was performed considering the hypothesis raised from the DSC results. Figure 2 shows the X-ray diffraction spectrum corresponding to the mixed carrageenan (κ and λ), TiO$_2$ NPs, and the different nanocomposites. The diffractogram shows a crystalline phase in the mixed carrageenan belonging to an inorganic salt, which some authors have reported as possibly potassium chloride (KCl).[22] For its part, Setijawati et al.[23] found an equal crystalline phase in different types of carrageenans (κ and ι) and attributed this crystalline structure to cohesive properties in these polysaccharides. However, these reflections matched very well with the phases of Sylvite (KCl) (95%) and Halite (NaCl) (5%) with card numbers 00-004-0587 and 01-089-3615 of the JCPDF, respectively. The appearance of the peaks corresponding to the nanoparticle phase of TiO$_2$ is observed from the concentration of 0.1 wt %, together with the phases of the inorganic salts belonging to the mixed carrageenan. These two phases are maintained until the nanocomposite 5 wt %, where the phases of the salts disappear by complement, while the phase of TiO$_2$ prevails completely. This behavior is to be expected since there is an increase in the concentration of TiO$_2$ nanoparticles. This phase of TiO$_2$ is in accordance with the card number (00-021-1276) of the JCPDF. This change in the intensity of the peaks indicates a concentration change in the samples due to the variation of TiO$_2$, which implied a change in the thermal properties observed in the DSC measurements. This structural and thermal change of the samples also imply possible changes occur in the different bonds in the nanocomposites. Therefore, infrared spectroscopy measurements were conducted for the mixed carrageenan (κ and λ), TiO$_2$ NPs, and the different nanocomposites.

3.3. Vibrations of Molecular Structures. It is important to know the oscillation modes (vibrations) of the carrageenan structure together with the TiO$_2$ NPs. Figure 3 shows the FT-IR spectrum for different nanocomposites and their respective precursors between 4000 and 400 cm^{-1} (graph A) and 1500 and 400 cm^{-1} (graph B). For mixed carrageenan, contributions are observed in the bands corresponding to both κ-carrageenan and λ-carrageenan, together with the common bands for both, showing more intensity for one type of carrageenan than for the other. In Figure 3A, the spectrum shows a band at 3392 and 3412 cm^{-1} that corresponds to the OH stretch vibrations, while the band at 1641 cm^{-1} corresponds to the water bound at the nanocomposites and at the TiO$_2$ NPs.[6,22−24] The most important region to identify the different carrageenan types is the region of the fingerprint, which corresponds to the spectrum between 1500 and 400 cm^{-1} (Figure 3B), where the
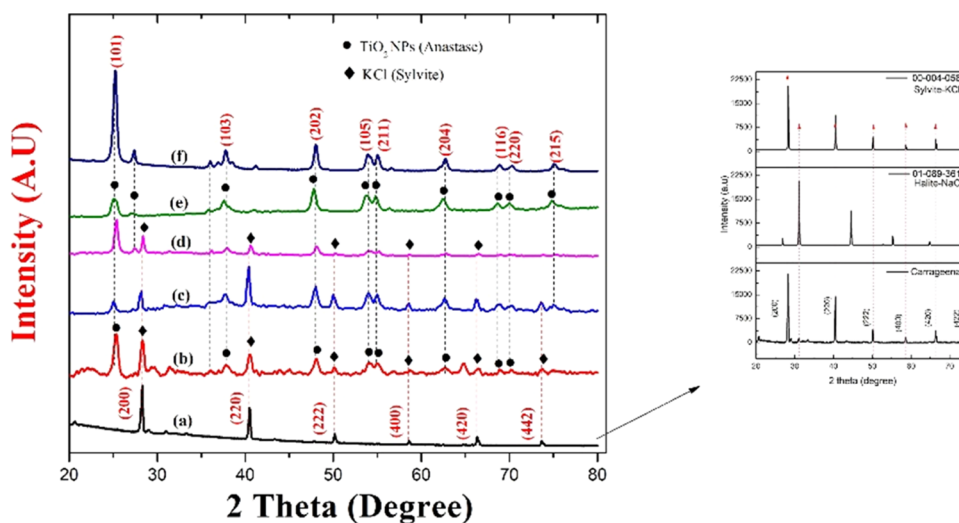
Figure 2. X-ray measurements for the different nanocomposites: (a) carrageenan (CR), (b) carrageenan with a concentration of 0.1 wt % of TiO_2 NPs (CR0.1%), (c) carrageenan with a concentration of 0.5 wt % of TiO_2 NPs (CR0.5%), (d) carrageenan with a concentration of 1 wt % of TiO_2 NPs (CR1%), (e) carrageenan with a concentration of 5 wt % of TiO_2 NPs (CR5%), and (f) pure TiO_2 NPs.
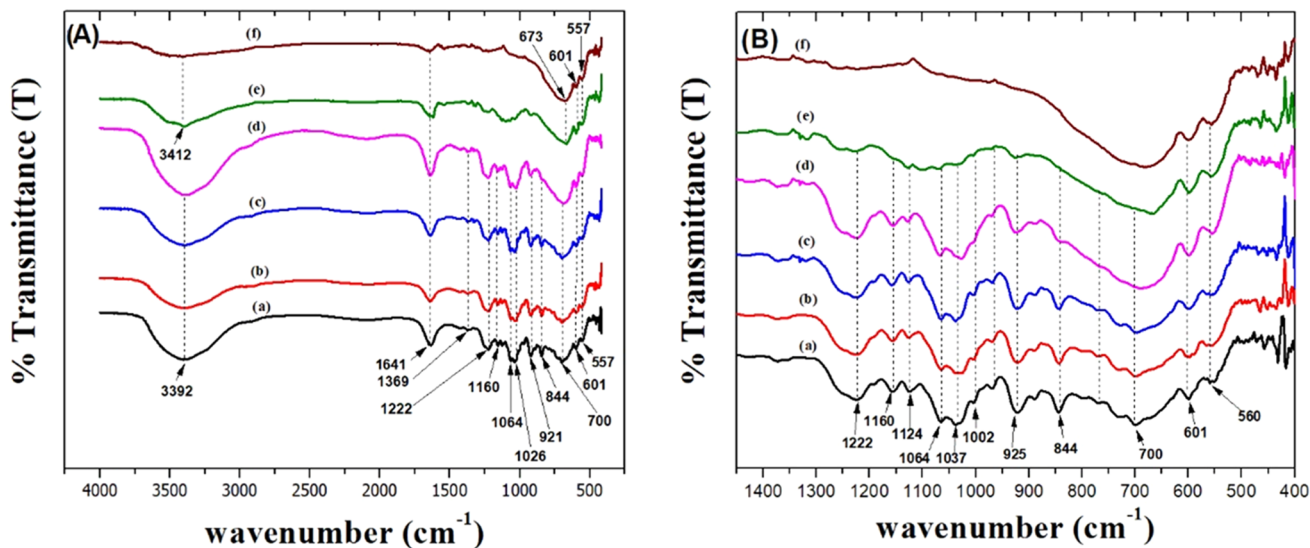
Figure 3. (A) Spectrum of FT-IR in the range of 4000−400 cm^{-1} and (B) spectrum in the range of the fingerprint (1400−400 cm^{-1}) for (a) carrageenan (CR), (b) carrageenan with a concentration of 0.1 wt % of TiO_2 NPs (CR0.1%), (c) carrageenan with a concentration of 0.5 wt % of TiO_2 NPs (CR0.5%), (d) carrageenan with a concentration of 1 wt % of TiO_2 NPs (CR1%), (e) carrageenan with a concentration of 5 wt % of TiO_2 NPs (CR5%), and (f) pure TiO_2 NPs.

band is observed at 1026 cm^{-1}, characteristic of the λ-carrageenan, while the bands at 844 and 731 cm^{-1} correspond to the κ-carrageenan.[6,22−26] The peak at 1222 cm^{-1} corresponds to O═S═O (asymmetric stretch) and is shown as a broad peak due to the contribution of these groups by the two carrageenan types (κ and λ). For its part, another characteristic band is the 925 cm^{-1} that belongs to the coupling of the stretching vibrations of the C−O−C in the 3,6-anhydrous-D-galactose (3,6-anhydrogalactose). In this same region of the fingerprint, there is a very particular behavior in the bands since there is a progressive decrease in its intensity as the percentage of nanoparticles of TiO_2 increases (0.1, 0.5, and 1 wt %) and a significant reduction in the intensity of the bands for the sample of 5 wt %, this due to the interaction of TiO_2 with the most external groups in the mixed carrageenan such as the glycosidic bonds in 1002 cm^{-1}, the vibrations of stretches of the C−O−C in 3,6-anhydrogalactose in 925 cm^{-1},

groups C4−O−S in galactose (stretch) in 844 cm^{-1}, groups C4−O−S in galactose (stretch) in 700 cm^{-1}, and the groups O═S═O (doubling) in 601 and 560 cm^{-1}. These last two bands do not show significant changes because they coincide with the bands belonging to the vibrations of the Ti−O groups (Table 1).[27]

3.4. Electrical Properties. Knowing the thermal and structural behavior of nanocomposites, it is also necessary to know the electrical properties that they present and determine which of them have a greater potential in the ethanol electro-oxidation processes. Figure 4 shows this electrical behavior in the Cole−Cole plot for carrageenan (CR) and the different nanocomposites (CR0.1%, CR0.5%, CR1%, and CR5%). In the region of high frequencies, there is a variation in the semicircle by the different samples as the concentration of TiO_2 nanoparticles increases. This variation of the semicircle may be related to ionic conduction in the bulk of the samples.

Table 1. Bands and Functional Groups Detected in Nanocomposite Samples Corresponding to κ and λ Carrageenan (+, Present; −, Absent)

wavenumber (cm^{-1})	functional group	κ-carrageenan	λ-carrageenan	references
3392	O−H (stretching)	+	+	6, 24
1641	polymer-bound water	+	+	6
1369	sulfates (stretching)	+	+	6, 24
1222	O=S=O (asymmetric stretching)	+	+	6, 7, 24, 28−31
1160	C−O−C (asymmetric stretching)	+	+	6, 24
1064	C−O + C−OH	+	+	6, 22
1026	S=O in C2 (pseudo-symmetric stretching)	−	+	6
1002	Glycosidic bonds	+	+	6
925	3,6-anhydro-D-galactose	+	+	26, 28, 31
844	C4−O−S group in galactose (stretching)	+	−	6, 24, 28−30
731	C−O−C α(1,3) (stretching)	+	−	6, 22
700	sulfates in C4, galactose	+	−	30
601	O=S=O (bending)	+	+	31
560	O=S=O (bending)	+	+	6, 22
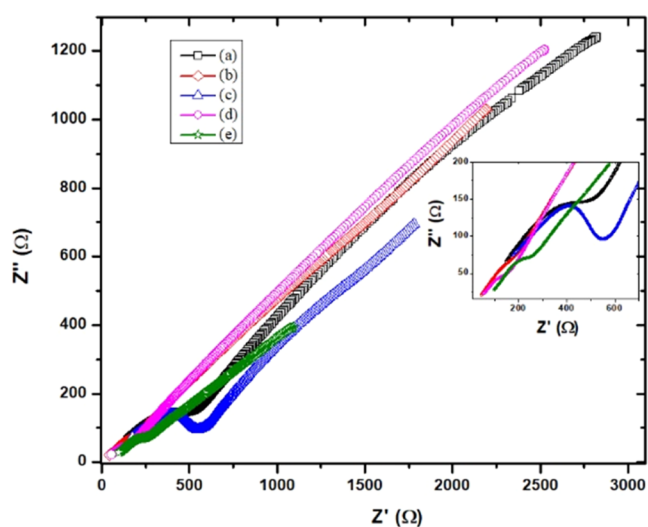
Figure 4. Cole−Cole graph of the electrical behavior for (a) carrageenan (CR), (b) carrageenan with a concentration of 0.1 wt % of TiO$_2$ NPs (CR0.1%), (c) carrageenan with a concentration of 0.5 wt % of TiO$_2$ NPs (CR0.5%), (d) carrageenan with a concentration of 1 wt % of TiO$_2$ NPs (CR1%), and (e) carrageenan with a concentration of 5 wt % of TiO$_2$ NPs (CR5%).

Table 2. Conductivity Values of Nanocomposites

samples	conductivity (S/cm)
CR	1.07×10^{-4}
CR0.1%	1.26×10^{-4}
CR0.5%	1.21×10^{-4}
CR1%	1.76×10^{-4}
CR5%	2.08×10^{-4}

In the region of low frequencies, there is an inclined spike that is attributed to the blocking effect by the electrodes.[32] In addition, the bulk resistance R_b was obtained through the intercept between the semicircle and inclined spike. With these resistance values, the ionic conductivity at room temperature was estimated from the following equation:

$$\sigma = \frac{t}{R_b A} \tag{1}$$

where t is the thickness of the membranes, R_b is the electrical resistance of the package, and A is the contact area of the electrodes. The obtained conductivity values are shown in Table 2. The ionic conductivity value for carrageenan (CR) is 1.07×10^{-4} S/cm, two orders of magnitude greater than that reported by Christopher et al.[33] and Liew et al.[34] for κ-carrageenan and an order of magnitude greater than that reported by Karthikeyan et al.[35] and Monihan et al.[36] for ι-carrageenan. This increase in conductivity values is due to traces of inorganic salts (KCl and NaCl) observed in X-ray measurements, which facilitate conduction through electrolytic polymers, as reported.[37] There is a tendency to increase the conductivity values in the samples as the concentration of TiO$_2$ nanoparticles increases, reaching its maximum in the CR5% nanocomposite of 2.08×10^{-4} S/cm. The addition of TiO$_2$ nanoparticles facilitates the movement of hydrogen protons through the polymer chains, which improves the conductivity of the membranes. However, there are variations in the conductivity values that can be attributed to the interaction of Ti$^+$ with OH groups of carrageenan, as we observe in the FTIR measurements. This decrease in conductivity values for higher concentrations of TiO$_2$ is attributed to the formation of clusters in the samples, as seen in the SEM images, which makes it difficult for the ions to pass through the bulk of nanocomposites.

3.4.1. Dielectric Study. It is known that the dielectric constant for many solids and liquids, in general, depends on the frequency. This dispersion phenomenon can be described by the complex dielectric constant through the following equation

$$\varepsilon^* = \varepsilon' - i\varepsilon'' \tag{2}$$

Where ε' is the real part of the complex dielectric constant or dielectric constant of the material and ε'' is the imaginary part of the complex dielectric constant or dielectric loss that is related to the energy dissipation processes. The variation of the dielectric constant and the dielectric loss with frequency is shown in Figure 5A,B, respectively, for the different nanocomposites. There is an increase in the dielectric constant value at low frequencies, and the dielectric loss decreases for higher frequencies until reaching a constant value. In addition, with the increase in the concentration of TiO$_2$ nanoparticles, there is an increase in the values of the dielectric constant and the dielectric loss until they reach a maximum value for the
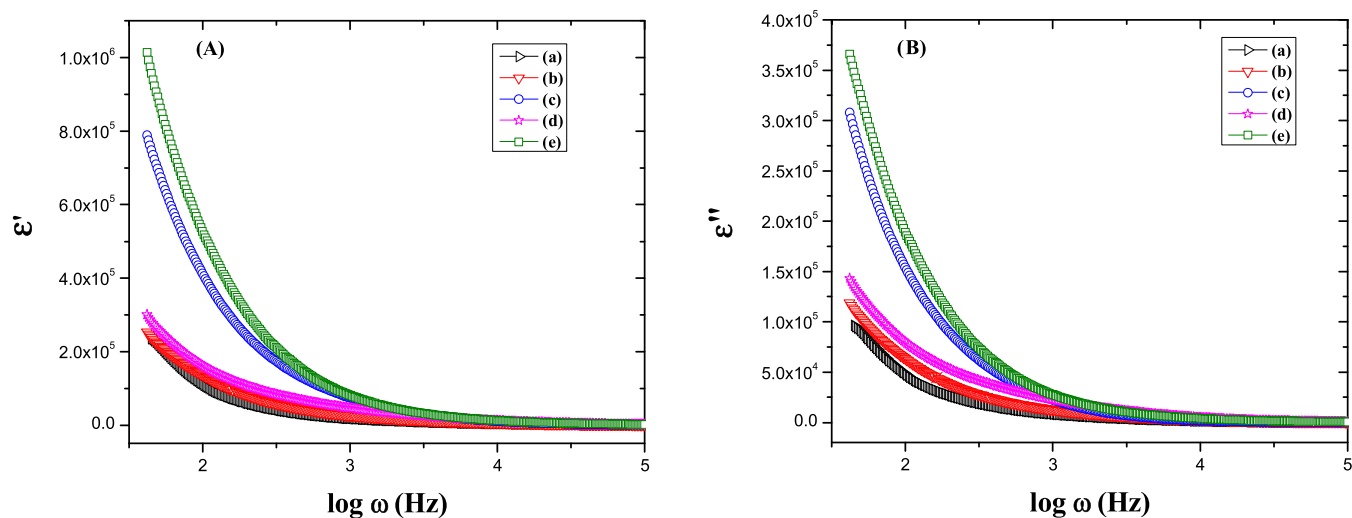
Figure 5. (A) Dielectric constant and (B) dielectric loss for (a) carrageenan (CR), (b) carrageenan with a concentration of 0.1 wt % of TiO_2 NPs (CR0.1%), (c) carrageenan with a concentration of 0.5 wt % of TiO_2 NPs (CR0.5%), (d) carrageenan with a concentration of 1 wt % of TiO_2 NPs (CR1%), and (e) carrageenan with a concentration of 5 wt % of TiO_2 NPs (CR5%) as a function of frequency.
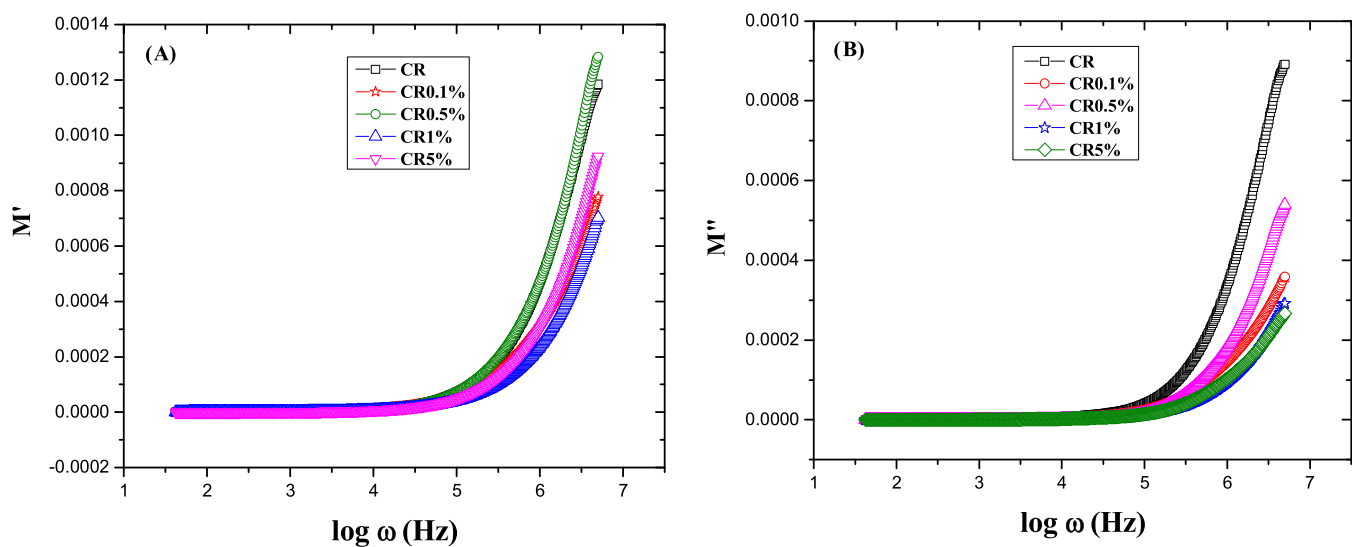
Figure 6. (A) Real and (B) imaginary parts of the electrical module for the carrageenan and the different nanocomposites as a function of frequency.
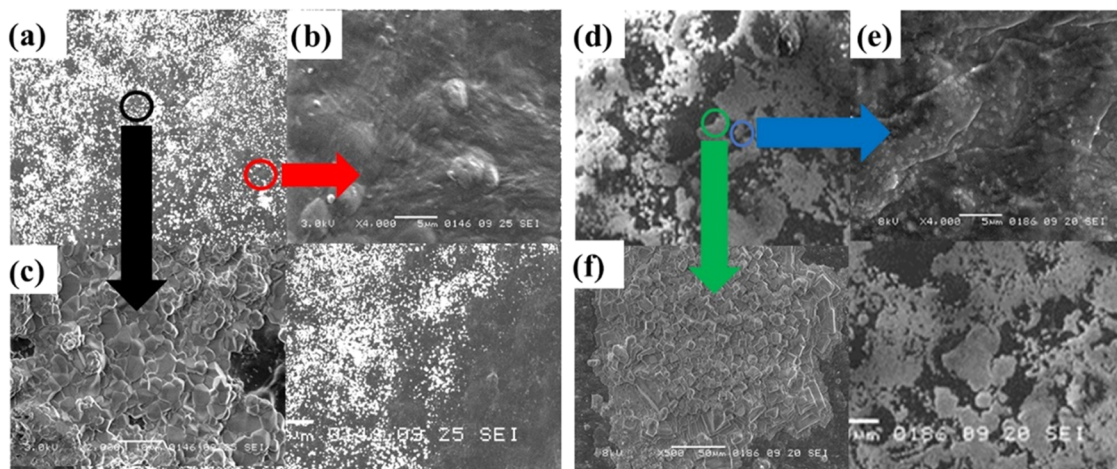
Figure 7. Micrographs. Panels (a–c) correspond to carrageenan (CR), while panels (d–f) correspond to carrageenan with a concentration of 0.1 wt % TiO_2 NPs (CR0.1%).
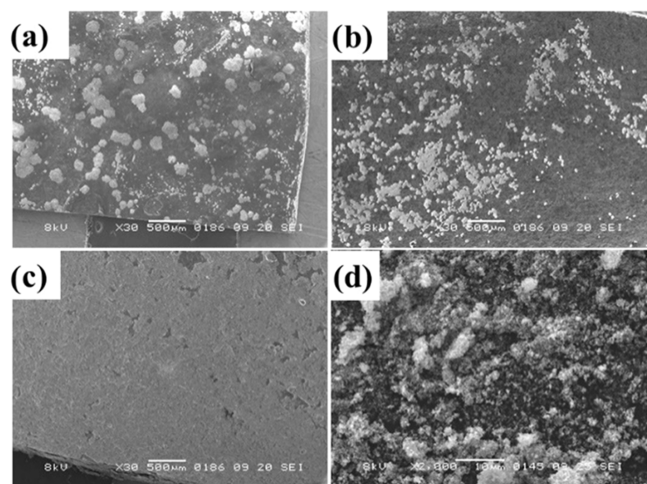
Figure 8. Micrographs of carrageenan with different concentrations of TiO_2 NPs: (a) 0.5 wt %, (b) 1 wt %, (c) 5 wt %, and (d) pure TiO_2 NPs.

CR5% sample, which is in accordance with the conductivity results. This increase could be due to the polarization effect of the dipoles, ions, and charge space in the samples close to the electrodes.[32] At high frequencies, the dipoles and ions cannot follow the frequency of the applied electric field, which reduces the charge accumulation in the electrode/electrolyte interface, causing the dielectric constant and the dielectric loss to decrease suddenly. These values of the dielectric constant for nanocomposites are in the same order of magnitude as those reported by Hema et al.,[32,38] making them good candidates for use in capacitors and fuel cells.

The complex electrical module is a vital magnitude to describe the phenomenon of ionic transport in materials and is expressed as follows

$$M^* = \frac{1}{\varepsilon^*} = M' - iM'' \tag{3}$$

M' and M'' are the real and imaginary parts of the complex electrical module. In Figure 6A,B, at low frequencies, a long tail is observed along with almost zero values for M' and M'' in all

nanocomposites. These two behaviors are associated with a high capacitance of the electrodes and negligible polarization on these at low frequencies.[32] At the end of the high-frequency region, there is an increase in both quantities (M' and M'') due to the bulk effects on the nanocomposites.

3.5. Morphology of the Samples. Figure 7A shows a low-magnification SEM micrograph of the surface of carrageenan (CR). The area enclosed by the red circle has an amorphous surface, typical of carrageenan, as shown in Figure 7B, while in Figure 7C, the area enclosed by the black circle presents cube-shaped agglomerates, which correspond to the inorganic salts KCl and NaCl, evidenced by the results of X-rays. On the other hand, Figure 7D shows the surface of carrageenan with a concentration of 0.1% of TiO_2 NPs (CR0.1%). The area enclosed by the blue circle has microclusters embedded in the surface belonging to the TiO_2 NPs, as shown in Figure 7E. In addition, Figure 7F shows the formation of large islands corresponding to the cube-shaped structure of inorganic salts.

On the other hand, Figure 8 shows low SEM micrographs of the carrageenan surface with different concentrations of TiO_2 NPs (0.5, 1, and 5%) and pure TiO_2 NPs. If we compare the CR0.5% sample (Figure 8A) with the CR (Figure 7A) and CR0.1% (Figure 7D) samples, we observe that the surface area covered by the large islands of cube-shaped structures has decreased. The structures are now limited to isolated islands. On the other hand, the number of microclusters has increased compared to Figure 7D. Figure 8B corresponds to carrageenan with a concentration of 1% of TiO_2 NPs (CR1%); in comparison, with samples CR, CR0.1%, and CR0.5%, cube structures are not observed, but an amorphous area, where the agglomeration of TiO_2 NPs into microclusters occurs, is observed. Figure 8C shows the nanocomposite with the highest concentration of TiO_2 NPs, 5% (CR5%), where the surface is almost completely covered by a continuous film of TiO_2 NPs. No structured cubes are observed, and the microclusters are limited to the smallest points. These results coincide with the X-ray measurements, where a progressive increase in the TiO_2 peaks was observed with a decrease in the phase corresponding to the inorganic salts (KCl and NaCl).
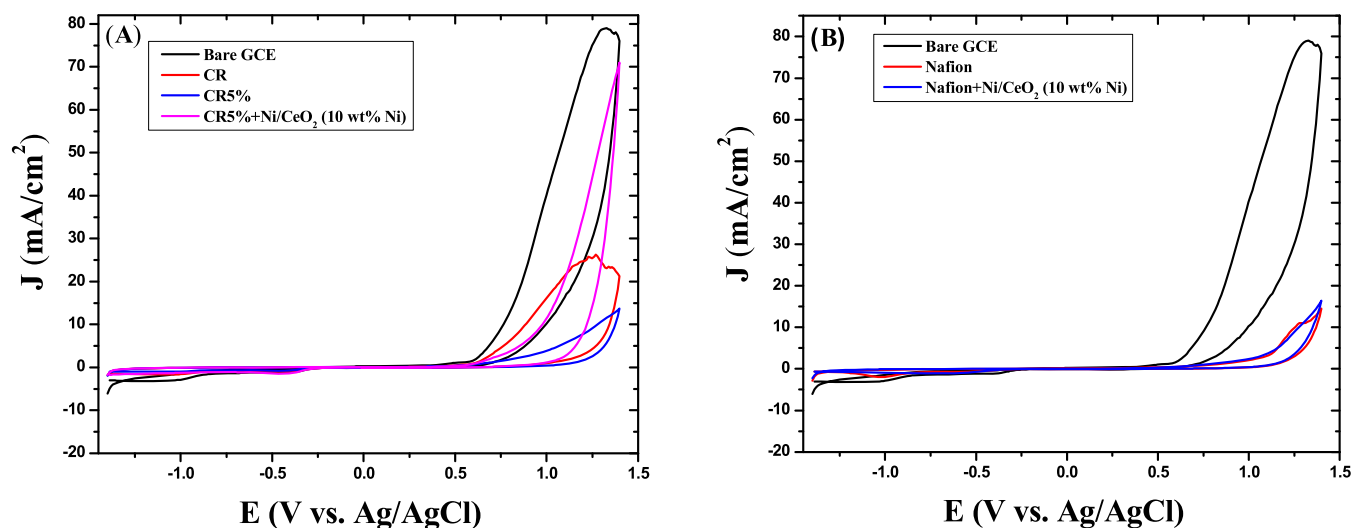
Figure 9. Cyclic voltammograms (A) for the glass carbon electrode (GCE), CR, CR5%, and CR5% + Ni/CeO$_2$ (10 wt % Ni) and (B) GCE, Nafion, and Nafion + Ni/CeO$_2$ (10 wt % Ni) in a solution of 1 M KOH at 100 mV/s.
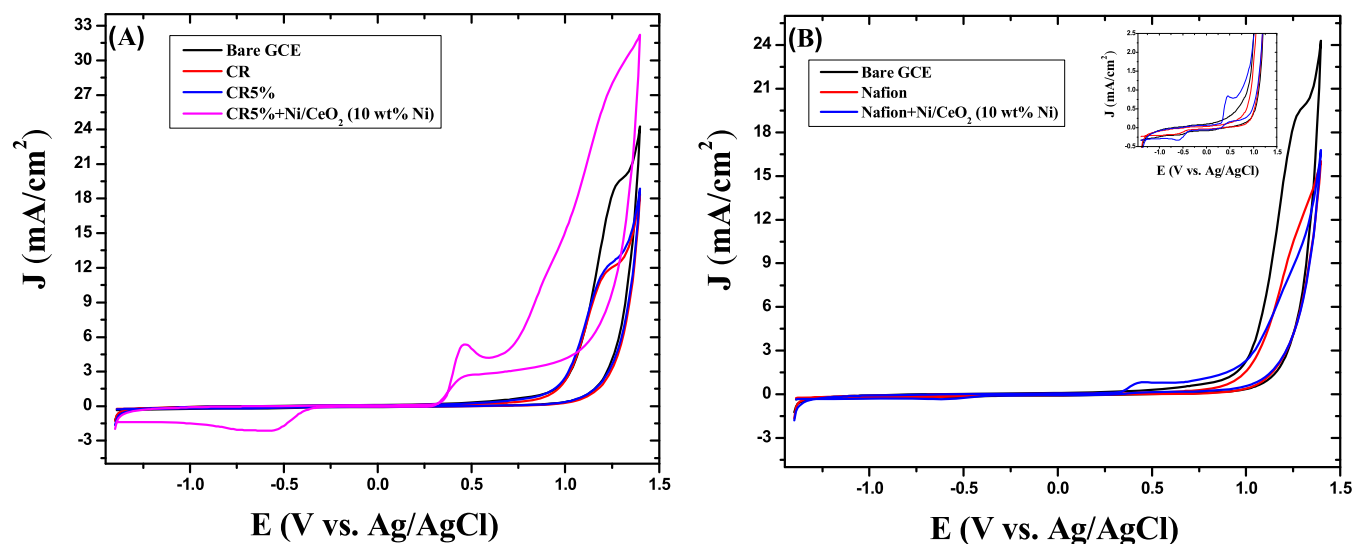
Figure 10. Cyclic voltammograms (A) GCE, CR, CR5%, and CR5% + Ni/CeO$_2$ (10 wt % Ni) and (B) GCE, Nafion, and Nafion + Ni/CeO$_2$ (10 wt % Ni) in a solution of 1 M KOH and 1 M ethanol at 100 mV/s.
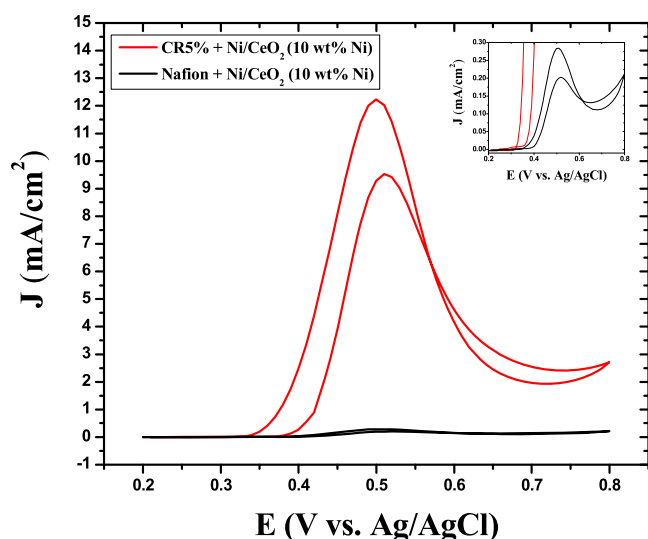
Figure 11. Cyclic voltammograms of CR5% + Ni/CeO$_2$ (10% wt Ni) and Nafion + Ni/CeO$_2$ (10% wt Ni) in a solution of 1 M KOH and 1 M ethanol at 100 mV/s.

On the other hand, Figure 8D corresponds to the pure TiO$_2$ NPs, where the microclusters were observed.

3.6. Cyclic Voltammetry Measurements (CV). The technique mostly used to determine the oxidation–reduction processes in different substances is cyclic voltammetry. Figure 9 shows cyclic voltammograms for the carbon fiber working electrode (GCE), the membranes of CR, CR5%, and CR5% mixed with Ni/CeO$_2$ (CR5% + Ni/CeO$_2$ (10% wt Ni)), and for GCE, Nafion and Nafion mixed with Ni/CeO$_2$ (Nafion + Ni/CeO$_2$ (10 wt % Ni)) at a scan rate of 100 mV/s in a range of −1.4 to 1.4 V in a 1 M KOH solution. These measurements show small reduction peaks for the GCE and the CR5% membrane mixed with Ni/CeO$_2$ (10 wt % Ni) (Figure 9A). Similarly, only shows a small reduction peak corresponding to the GCE (Figure 9B).

3.6.1. Ethanol Oxidation. The performance of the membranes in an alkaline medium (KOH) was evaluated for ethanol oxidation using cyclic voltammetry measurements.

Figure 10 shows two cyclic voltammograms for the working carbon electrode (GCE), the CR, CR5%, and CR5% membranes mixed with Ni/CeO$_2$ (CR5% + Ni/CeO$_2$ (10 wt % Ni)), and for the GCE, the Nafion and the Nafion mixed with Ni/CeO$_2$ (Nafion + Ni/CeO$_2$ (10 wt % Ni)) at a scan rate of 100 mV/s over a range of −1.4 to 1.4 V in a solution of 1 M KOH and 1 M ethanol. Figure 10A shows two peaks of the current density that correspond to the oxidation of ethanol around 0.35 V and one reduction peak around −0.35 V by the CR5% membrane mixed with Ni/CeO$_2$. Similarly, Figure 10B shows two small oxidation peaks around 0.35 V and one reduction peak around −0.35 V, corresponding to Nafion mixed with Ni/CeO$_2$. These voltammograms show the synergy between the CR5% membrane, Nafion, and Ni/CeO$_2$ in oxidizing ethanol. However, the current density peaks show greater intensity with the CR5% membrane.

To better study this behavior, measurements were conducted in the voltage range between 0.2 and 0.8 V, which includes the two oxidation peaks by the membranes, as shown in Figure 11, where the cyclic voltammograms of the membranes are compared for CR5% + Ni/CeO$_2$ (10 wt % Ni) and Nafion + Ni/CeO$_2$ (10 wt % Ni) in a solution of 1 M KOH and 1 M ethanol at a scan rate of 100 mV/s. These results show a significant increase (40 times greater) in the current density peaks corresponding to the oxidation of ethanol by the CR5% sample with respect to the Nafion sample. The increase in the peak current density in the CV measurement is due to the adsorption of the ethoxy groups on the surface of the CR5% and the Ni/CeO$_2$ membranes on the working electrode, around 0.35 V, reaching its maximum value of 9.52 mA/cm^2 at 0.50 V on the forward scan voltage. In the reverse scan voltage, we observe a second ethanol oxidation peak at a current density of 12.22 mA/cm^2, which is due to the adsorption of the ethoxy groups of fresh ethanol on the surface of CR5% and Ni/CeO$_2$. These values in the peak current density are higher than those reported by Yang et al.[39] for the electro-oxidation of ethanol through bimetallic PtPb nanoparticles on a graphene–Nafion film, whose values are 7.69, 2.28, and 0.56 mA/cm^2 for PtPd/Nf–graphene/GCE, Pt/Nf–graphene/GCE, and the Pd/Nf–graphene/GCE, respectively.
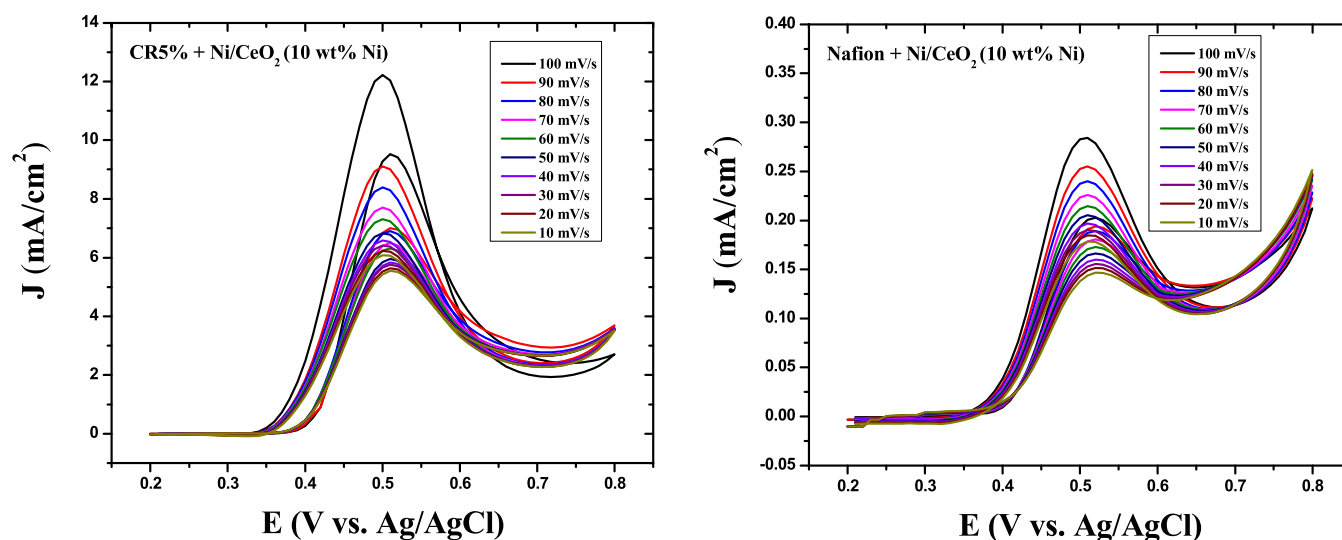
Figure 12. Cyclic voltammograms of CR5% + Ni/CeO$_2$ (10 wt % Ni) and Nafion + Ni/CeO$_2$ (10 wt % Ni) at different scan rates from 10 to 100 mV/s in a solution of 1 M KOH and 1 M ethanol.
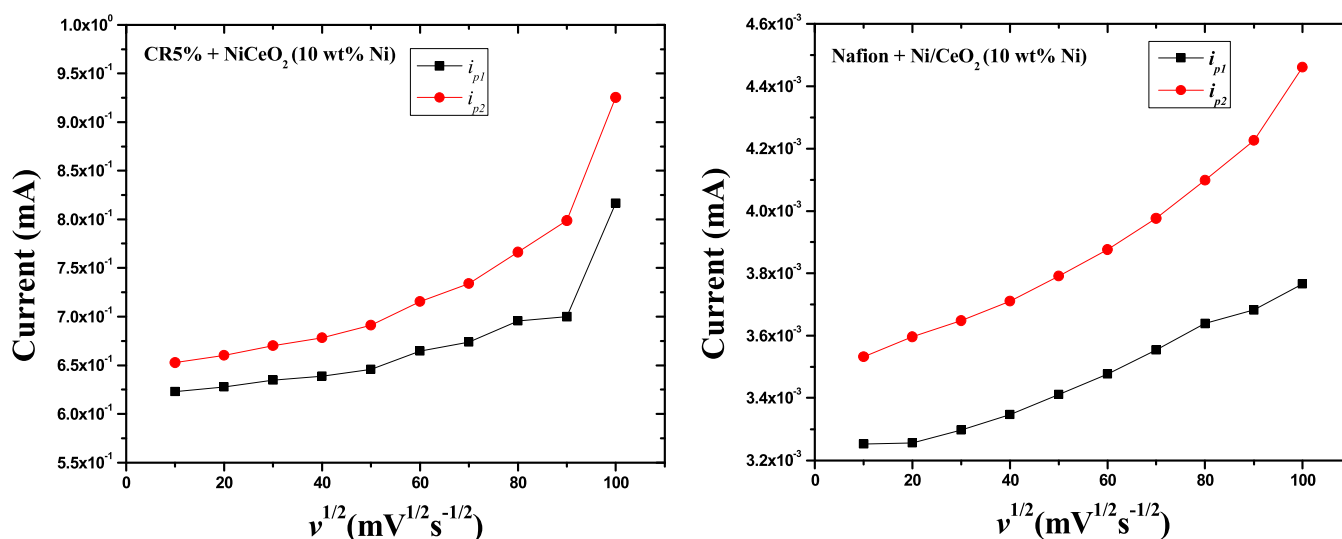
Figure 13. Graphs of current vs square root of scan rate for CR5% + Ni/CeO$_2$ (10 wt % Ni) and Nafion + Ni/CeO$_2$ (10 wt % Ni).

When comparing the values of the peak current densities between CR5% + Ni/CeO$_2$ and Nafion + Ni/CeO$_2$, it is observed that there are significant differences among the systems (Figure 11). This difference in peak current density could be associated with the formation of a surface with a higher amount of oxygen vacancies for CR5% + Ni/CeO$_2$, resulting in a higher amount of reduced metal cations (Ti$^+$, Ce$^+$), possibly facilitating the anchoring of ethoxy groups on the electrode surface.[40] Contrary to Nafion + Ni/CeO$_2$, which only have C−F and S═O groups in the working electrode, the availability of reduced metal cations is limited for the anchoring of the ethoxy groups on the electrode surface, thus resulting in a small density of current (Figure 11).

Figure 12 shows the measurements for different speeds (10−100 mV/s) for CR5% + Ni/CeO$_2$ (10 wt % Ni) and Nafion + Ni/CeO$_2$ (10 wt % Ni). The progressive increase in the peak current density is observed as the scan rate increases, which demonstrates the direct proportionality relationship between the peak currents and the square root of the corresponding scan rate. This direct proportionality relationship is shown in

Figure 13 as straight lines with a positive slope for the different peak currents, both for the CR5% + Ni/CeO$_2$ and the Nafion + Ni/CeO$_2$ membranes, respectively.

Another important characteristic in CV measurements is the number of cycles to which a sample is subjected. Figure 14 shows the measurements at 50 mV/s for CR5% + Ni/CeO$_2$ and Nafion + Ni/CeO$_2$. The progressive decrease of the peak current density can be observed according to the number of cycles (20−60 cycles). The relative instability of the ethanol oxidation current density over the different cycles seems to suggest that there is a poisoning of the surface by reaction intermediates for both samples.

3.7. Energy Dispersive X-ray Spectroscopy (EDX). Continuing with the process of characterization of the membranes, it is necessary to study the chemical composition and the relative abundance of the elements that make them up. For this reason, EDX measurements were conducted, as shown in Figure 15, for each of the different membranes (CR, CR0.1%, CR0.5%, CR1%, and CR5%). In the CR0.1% membrane, we noticed main peaks corresponding to the S,
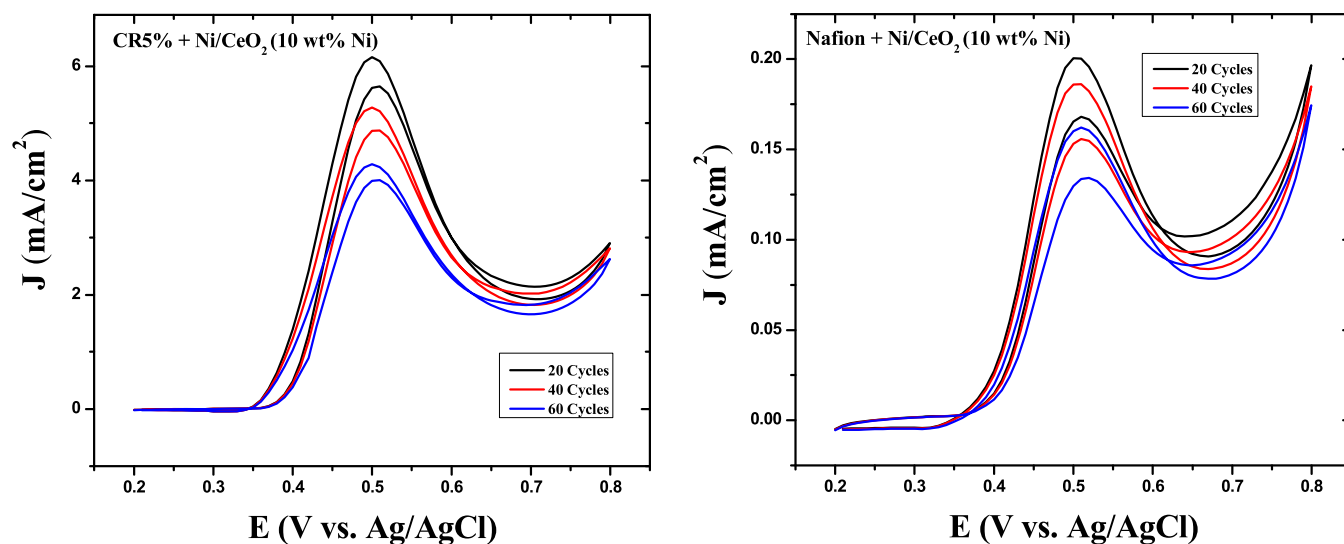
Figure 14. Cyclic voltammograms for different cycles (20 to 60) of CR5% + Ni/CeO$_2$ (10 wt % Ni) and Nafion + Ni/CeO$_2$ (10 wt % Ni) at a scan rate of 50 mV/s in a solution of 1 M KOH and 1 M ethanol.
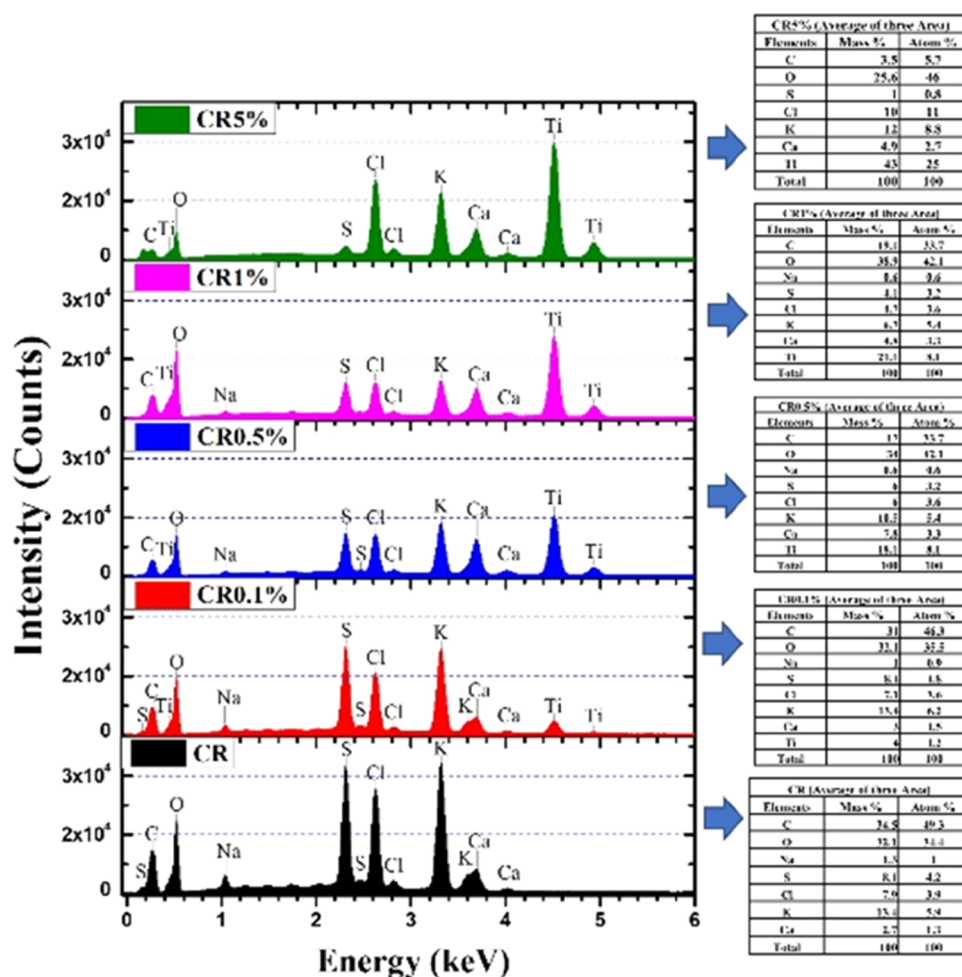
Figure 15. EDX measurements for different samples.

O, and C elements that are the main components of the polysaccharide structure (κ-carrageenan and λ-carrageenan), which are present in all membranes, while the peaks corresponding to the K, Cl, Na, and Ca ions belong to inorganic salts, which are found in commercial carrageenan.[41]

These peaks of the inorganic salts were also found in the XRD measurements (see Figure 2). When we start to dope the CR membrane with different concentrations of TiO$_2$ NPs, we can see the appearance of the Ti element in the CR0.1% membrane around 0.46, 4.52, and 4.94 keV. For these last

two energy values, its progressive increase in intensity is observed, as the TiO$_2$ NP concentration increases, until it reaches its maximum value in the CR5% membrane.

4. CONCLUSIONS

Using an environmentally friendly method (solvent evaporation), carrageenan nanocomposites were synthesized with different concentrations of TiO$_2$ NPs. In the DSC studies, the thermal behavior of the nanocomposites was observed, where there was a reduction in the decomposition temperature (~200 °C) with the increase in the concentration of TiO$_2$ NPs. This increase in concentration is evidenced in the XRD measurements with the appearance of the TiO$_2$ NPs and the progressive disappearance of traces of inorganic salts (KCl and NaCl) in the nanocomposites, as well as the reduction of the intensity in some of the peaks in the FTIR spectra corresponding to κ-carrageenan and λ-carrageenan. The conductivity of the ionic species was confirmed through impedance measurements, giving a maximum value of 2.08 × 10^{-4} S/cm for the CR5% membrane. SEM micrographs showed the formation of microclusters by TiO$_2$ NPs and islets belonging to the inorganic salts in the nanocomposites. In addition, through EDX measurements, the presence of TiO$_2$ NPs and inorganic salts was corroborated. In the electrochemical measurements, the CR5% + Ni/CeO$_2$ showed excellent values of 9.22 and 12.22 mA/cm^2 in forward and reverse peak current density, respectively, which demonstrates its efficiency in the electro-oxidation of ethanol compared with commercial Nafion membranes (Nafion + Ni/CeO$_2$). We have demonstrated through the combination of synthesis, characterization, and cyclic voltammetry measurements that CR5% + Ni/CeO$_2$ membranes are a viable alternative for the manufacture of electrodes for the electro-oxidation of ethanol in alkaline medium, with potential application in direct alcohol fuel cells (DAFC).

■ AUTHOR INFORMATION

Corresponding Authors

Ermides Chavez-Baldovino − *Department of Physics, University of Puerto Rico-Rio Piedras, San Juan 00925-2537, Puerto Rico*; Email: ermides.chavez@upr.edu

Liz M. Díaz-Vázquez − *Department of Chemistry, University of Puerto Rico-Rio Piedras, San Juan 00925-2537, Puerto Rico*; ● orcid.org/0000-0002-6285-0102; Email: liz.diaz2@upr.edu

Authors

Carlos A. Malca-Reyes − *Department of Physics, University of Puerto Rico-Rio Piedras, San Juan 00925-2537, Puerto Rico*

Roberto Masso − *Department of Physics, University of Puerto Rico-Rio Piedras, San Juan 00925-2537, Puerto Rico*

Peter Feng − *Department of Physics, University of Puerto Rico-Rio Piedras, San Juan 00925-2537, Puerto Rico*

Adrian Camacho − *Department of Physics, University of Puerto Rico-Rio Piedras, San Juan 00925-2537, Puerto Rico*

Janeth Sarmiento − *Instituto de Ciencias BUAP, Benemérita Universidad Autónoma de Puebla, Puebla 72530, México*

Justin I. Borrero Negrón − *Department of Chemical Engineering, University of Puerto Rico, Mayagüez 00681-9000, Puerto Rico*

Yomaira J. Pagán-Torres − *Department of Chemical Engineering, University of Puerto Rico, Mayagüez 00681-9000, Puerto Rico*; ● orcid.org/0000-0002-8655-7058

Complete contact information is available at:
https://pubs.acs.org/10.1021/acsomega.3c01188

Author Contributions

All authors contributed to the completion of this article and participated in the design, execution, analysis, and writing of the manuscript. Ermides Chavez-Baldovinio synthesized the nanocomposites, performed some characterizations, analyzed part of the data, and wrote this manuscript; Carlos A. Malca-Reyes contributed to the revision of the manuscript; Roberto Masso carried out the impedance spectroscopy measurements and part of the data analysis; Adrian Camacho performed the SEM micrographs and part of their analysis; Janeth Sarmiento contributed to the analysis of some XRD spectra; Justin I. Borrero Negrn synthesized the Ni/CeO$_2$ (10 wt % Ni) sample; Liz M. Daz-Vasquéz, Yomaira J. Pagn-Torres, and Peter Feng edited and reviewed this manuscript, along with supervision and acquisition of funds to develop this research.

Notes

The authors declare no competing financial interest.

■ ACKNOWLEDGMENTS

■ REFERENCES

(1) Srivastava, N.; Chandra, S. Studies on a New Proton Conducting Polymer System: Poly (Ethylene Succinate) + NH4ClO4. *Eur. Polym. J.* **2000**, *36*, 421−433.

(2) Rani, M.; Rani, A.; Rudhziah, S.; Ahmad, A.; Mohamed, N. S. Biopolymer Electrolyte Based on Derivatives of Cellulose from Kenaf Bast Fiber. *Polymers* **2014**, *6*, 2371−2385.

(3) Thakur, V. K.; Thakur, M. K.; Raghavan, P.; Kessler, M. R. Progress in Green Polymer Composites from Lignin for Multifunctional Applications: A Review. *ACS Sustainable Chem. Eng.* **2014**, *2*, 1072−1092.

(4) Lizundia, E.; Urruchi, A.; Vilas, J. L.; León, L. M. Increased Functional Properties and Thermal Stability of Flexible Cellulose Nanocrystal / ZnO Films. *Carbohydr. Polym.* **2016**, *136*, 250−258.

(5) Vijaya, N.; Selvasekarapandian, S.; Sornalatha, M.; Sujithra, K. S.; Monisha, S. Proton-Conducting Biopolymer Electrolytes Based on Pectin Doped with NH 4 X (X = Cl, Br). *Ionics* **2016**, *23*, 2799−2808.

(6) Prado-Fernández, J.; Rodríguez-Vázquez, J. A.; Tojo, E.; Andrade, J. M. Quantitation of κ-, ι- and λ-Carrageenans by Mid-Infrared Spectroscopy and PLS Regression. *Anal. Chim. Acta* **2003**, *480*, 23−37.

(7) Belton, P. S.; Wilson, R. H.; Chenery, D. Interaction of Group I Cations with Iota and Kappa Carrageenans Studied by Fourier Transform Infrared Spectroscopy. *Int. J. Biol. Macromol.* **1986**, *8*, 247−251.

(8) Shajudheen, V. M..; Viswanathan, K; Rani, K. A.; Maheswari, A. U.; Kumar, S. S. A Simple Chemical Precipitation Method Of Titanium Dioxide Nanoparticles Using Polyvinyl Pyrrolidone as a

Capping Agent and Their Characterization. *Int. J. Chem. Mol. Eng.* **2016**, *10*, 556−559.

(9) Marinescu, C.; Sofronia, A.; Rusti, C.; Piticescu, R.; Badilita, V.; Vasile, E.; Baies, R.; Tanasescu, S. DSC Investigation of Nanocrystalline TiO2powder. *J. Therm. Anal. Calorim.* **2011**, *103*, 49−57.

(10) Lizundia, E.; Vilas, J. L.; León, L. M. Crystallization, Structural Relaxation and Thermal Degradation in Poly(l-Lactide)/Cellulose Nanocrystal Renewable Nanocomposites. *Carbohydr. Polym.* **2015**, *123*, 256−265.

(11) Shukur, M. F.; Ithnin, R.; Kadir, M. F. Z. Electrochimica Acta Electrical Characterization of Corn Starch-LiOAc Electrolytes and Application in Electrochemical Double Layer Capacitor. *Electrochim. Acta* **2014**, *136*, 204−216.

(12) Ng, C. A.; Camacho, D. H. Polymer Electrolyte System Based on Carrageenan-Poly (3, 4- Ethylenedioxythiophene) (PEDOT) Composite for Dye Sensitized Solar Cell. *IOP Conf. Ser.: Mater. Sci. Eng.* **2015**, *79*, No. 012020.

(13) Jo, S.; Oh, Y.; Park, S.; Kan, E.; Lee, S. H. Cellulose / Carrageenan / TiO 2 Nanocomposite for Adsorption and Photo-degradation of Cationic Dye. *Biotechnol. Bioprocess Eng.* **2017**, *22*, 734−738.

(14) Frühwirt, P.; Kregar, A.; Törring, J. T.; Katrašnik, T.; Gescheidt, G. Holistic Approach to Chemical Degradation of Nafion Membranes in Fuel Cells: Modelling and Predictions. *Phys. Chem. Chem. Phys.* **2020**, *22*, 5647−5666.

(15) Kurwadkar, S.; Dane, J.; Kanel, S. R.; Nadagouda, M. N.; Cawdrey, R. W.; Ambade, B.; Struckhoff, G. C.; Wilkin, R. Per- and Polyfluoroalkyl Substances in Water and Wastewater: A Critical Review of Their Global Occurrence and Distribution. *Sci. Total Environ.* **2022**, *809*, No. 151003.

(16) Bonato, M.; Corrà, F.; Bellio, M.; Guidolin, L.; Tallandini, L.; Irato, P.; Santovito, G. Pfas Environmental Pollution and Antioxidant Responses: An Overview of the Impact on Human Field. *Int. J. Environ. Res. Public Health* **2020**, *17*, No. 8020.

(17) Mullins, D. R. The Surface Chemistry of Cerium Oxide. *Surf. Sci. Rep.* **2015**, *70*, 42−85.

(18) Xi, Y.; Yang, W.; Ammal, S. C.; Lauterbach, J.; Pagan-Torres, Y.; Heyden, A. Mechanistic Study of the Ceria Supported, Re-Catalyzed Deoxydehydration of Vicinal OH Groups *Catal. Sci. Technol.* 8 5750 5762 DOI: 10.1039/c8cy01782d.

(19) Feliciano-Ramos, I.; Ortiz-Quiles, E. O.; Cunci, L.; Díaz-Cartagena, D. C.; Resto, O.; Cabrera, C. R. Unsupported Palladium Nanoparticles for Ethanol Cyclic Voltammetric Sensing in Alkaline Media. *J. Solid State Electrochem.* **2016**, *20*, 1011−1017.

(20) Tanaka, T.; Lu, T.; Yuasa, S.; Yamaura, K. Structure and Properties of Poly(Vinyl Alcohol)/k-Carrageenan Blends. *Polym. Int.* **2001**, *50*, 1103−1108.

(21) Prasad, K.; Kaneko, Y.; Kadokawa, J. I. Novel Gelling Systems of κ-, ι - and λ- Carrageenans and Their Composite Gels with Cellulose Using Ionic Liquid. *Macromol. Biosci.* **2009**, *9*, 376−382.

(22) Wei, J.; Liew, Y.; Loh, K. S.; Ahmad, A.; Lim, K. L.; Wan, W. R. M. Synthesis and Characterization of Modified κ -Carrageenan for Enhanced Proton Conductivity as Polymer Electrolyte Membrane. *Plos One* **2017**, *12*, No. e0185313.

(23) Setijawati, D. Carrageenan from Eucheuma Sp and Concentration Difference as Encapsulation Material toward Lactobacillus Acidophilus Viability at Simulation GI Tract PH Condition. *J. Basic Appl. Sci. Res.* **2014**, *4*, 261−268.

(24) Şen, M.; Erboz, E. N. Determination of Critical Gelation Conditions of κ-Carrageenan by Viscosimetric and FT-IR Analyses. *Food Res. Int.* **2010**, *43*, 1361−1364.

(25) Taylor, P.; Fan, L.; Peng, K.; Li, M.; Wang, L.; Wang, T. Preparation and Properties of Carboxymethyl κ -Carrageenan / Alginate Blend Fibers. *J. Biomater. Sci., Polym. Ed.* **2013**, *24*, 1099−1111.

(26) Mobarak, N. N.; Jumaah, F. N.; Ghani, M. A.; Abdullah, M. P.; Ahmad, A. Carboxymethyl Carrageenan Based Biopolymer Electrolytes. *Electrochim. Acta* **2015**, *175*, 224−231.

(27) Agarwal, S.; Saraswat, Y. K.; Saraswat, V. K. Synthesis and Thermal Characterization of Titanium-Dioxide Filled Polycarbonate/Polystyrene Blend Nanocomposites. *Macromol. Symp.* **2015**, *357*, 70−73.

(28) Mobarak, N. N.; Ramli, N.; Ahmad, A.; Rahman, M. Y. A. Chemical Interaction and Conductivity of Carboxymethyl κ-Carrageenan Based Green Polymer Electrolyte. *Solid State Ionics* **2012**, *224*, 51−57.

(29) Fan, L.; Peng, K.; Li, M.; Wang, L.; Wang, T. Preparation and Properties of Carboxymethyl κ -Carrageenan / Alginate Blend Fibers. *J. Biomater. Sci., Polym. Ed.* **2013**, *24*, 1099−1111.

(30) Daud, J. M.; Warzukni, N. S.; Salim, R. M.; Zuberdi, A. M. Semi-Refined κ-Carrageenan: Part 1. Chemical Modification of Semi-Refined κ-Carrageenan via Graft Copolymerization Method, Optimization Process and Characterization of Its Super Absorbent Hydrogel. *Orient. J. Chem.* **2015**, *31*, 973−980.

(31) Pereira, L.; Sousa, A.; Coelho, H.; Amado, A. M.; Ribeiro-Claro, P. J. A. Use of FTIR, FT-Raman And13C-NMR Spectroscopy for Identification of Some Seaweed Phycocolloids. *Biomol. Eng.* **2003**, *20*, 223−228.

(32) Hema, M.; Selvasekarapandian, S.; Arunkumar, D.; Sakunthala, A.; Nithya, H. Author' s Personal Copy FTIR, XRD and Ac Impedance Spectroscopic Study on PVA Based Polymer Electrolyte Doped with NH 4 X (X = Cl, Br, I). *J. Non Cryst. Solids* **2009**, *355*, 84−90.

(33) Christopher Selvin, P.; Perumal, P.; Selvasekarapandian, S.; Monisha, S.; Boopathi, G.; Chandra, M. V. L. Study of Proton-Conducting Polymer Electrolyte Based on K-Carrageenan and NH 4 SCN for Electrochemical Devices. *Ionics* **2018**, *24*, 3535−3542.

(34) Liew, J.; Loh, K.; Lim, K.; Daud, W. W. Effect of Modified Natural Filler O-Methylene Phosphonic -k-Carrageenan on Chitosan-Based Polymer Electrolytes. *Energies* **2018**, No. 1910.

(35) Karthikeyan, S.; Selvasekarapandian, S.; Premalatha, M.; Monisha, S.; et al. Proton-Conducting I-Carrageenan-Based Biopolymer Electrolyte for Fuel Cell Application. *Ionics* **2017**, *23*, 2775−2780.

(36) Moniha, V.; Alagar, M.; Selvasekarapandian, S.; Sundaresan, B.; Boopathi, G. Conductive Bio-Polymer Electrolyte Iota-Carrageenan with Ammonium Nitrate for Application in Electrochemical Devices. *J. Non-Cryst. Solids* **2018**, *481*, 424−434.

(37) Ahmad, N. H.; Isa, M. I. N. Structural and Ionic Conductivity Studies of CMC Based Polymer Electrolyte Doped with NH 4 Cl. *Adv. Mat. Res.* **2015**, *1107*, 247−252.

(38) Moniha, V.; Alagar, M.; Selvasekarapandian, S.; Sundaresan, B.; Hemalatha, R.; Boopathi, G. Synthesis and Characterization of Bio-Polymer Electrolyte Based on Iota-Carrageenan with Ammonium Thiocyanate and Its Applications. *J. Solid State Electrochem.* **2018**, *22*, 3209−3223.

(39) Yang, X.; Yang, Q.; Xu, J.; Lee, C. S. Bimetallic PtPd Nanoparticles on Nafion-Graphene Film as Catalyst for Ethanol Electro-Oxidation. *J. Mater. Chem.* **2012**, *22*, 8057−8062.

(40) Guchhait, S. K.; Paul, S. Development of Inexpensive High Energetic Electrodes Ni-Cu and Ni-CeO2-Cu for Renewable Energy through Direct Ethanol Fuel Cell. *J. Electrochem. Sci. Technol.* **2016**, *7*, 190−198.

(41) Bantang, J. P. O.; Bigol, U. G.; Camacho, D. H. Gel and Film Composites of Silver Nanoparticles in κ-, ι-, and λ-Carrageenans: One-Pot Synthesis, Characterization, and Bioactivities. *Bionanoscience* **2021**, *11*, 53−66.